Supporting information

Highly Stable Zn Metal Anode Enabled by Atomic Layer Deposited Al_2O_3 Coating for Aqueous Zinc-ion Batteries

Huibing He,[a] Huan Tong,[b] Xueyang Song,[a] Xiping Song[b], Jian Liu[a,*]

[a] *School of Engineering, Faculty of Applied Science, The University of British Columbia, Kelowna, BC V1V 1V7 Canada*

[b] *State Key Laboratory for Advanced Metals and Materials, University of Science and Technology Beijing, Beijing 100083, PR China*

[*] Corresponding author: jian.liu@ubc.ca (Jian Liu).

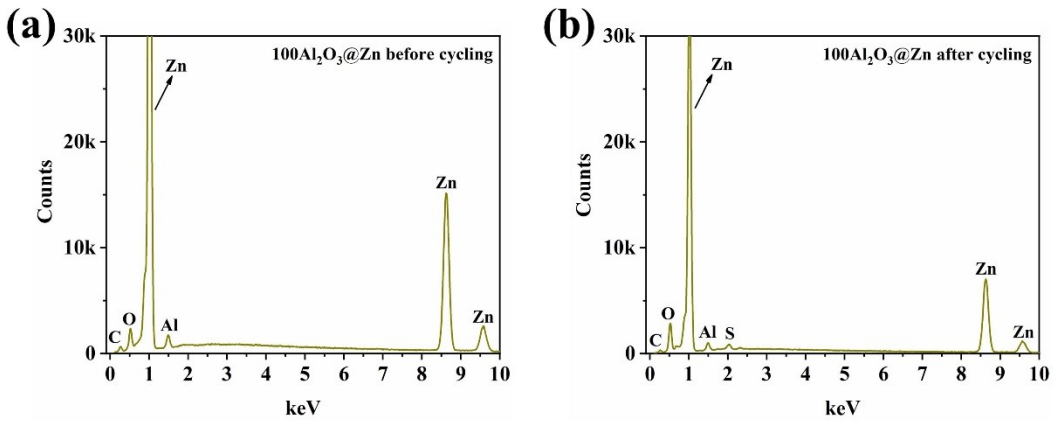

Figure S1. EDX spectra of $100Al_2O_3$@Zn before (a) and after (b) cycling.

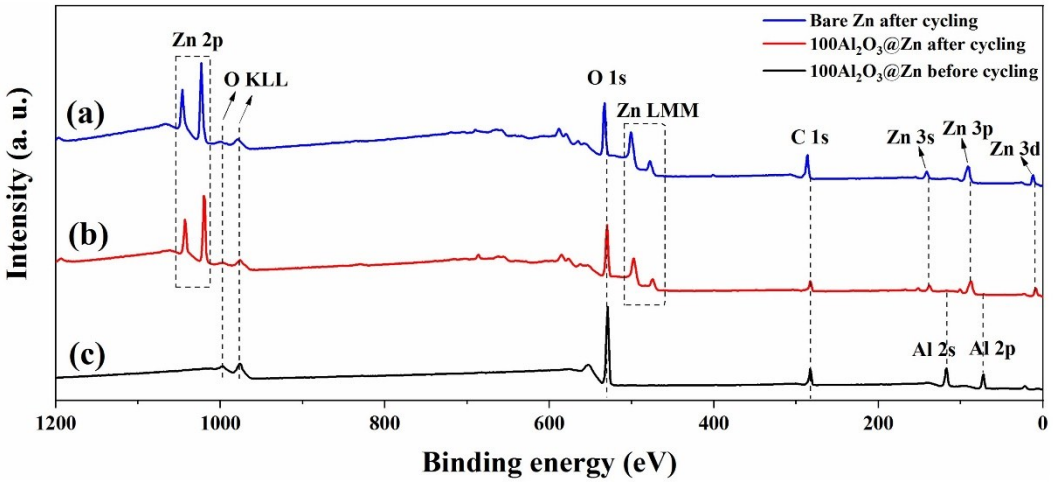

Figure S2. XPS survey spectra of bare Zn after cycling (a), $100Al_2O_3$@Zn after cycling (b) and $100Al_2O_3$@Zn before cycling (c).

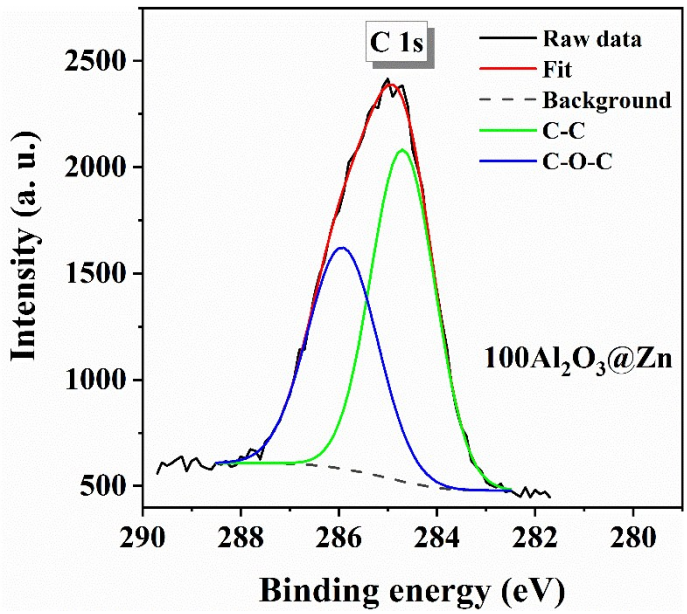

Figure S3. High resolution XPS spectra of C 1s core levels for $100Al_2O_3$ before cycling.

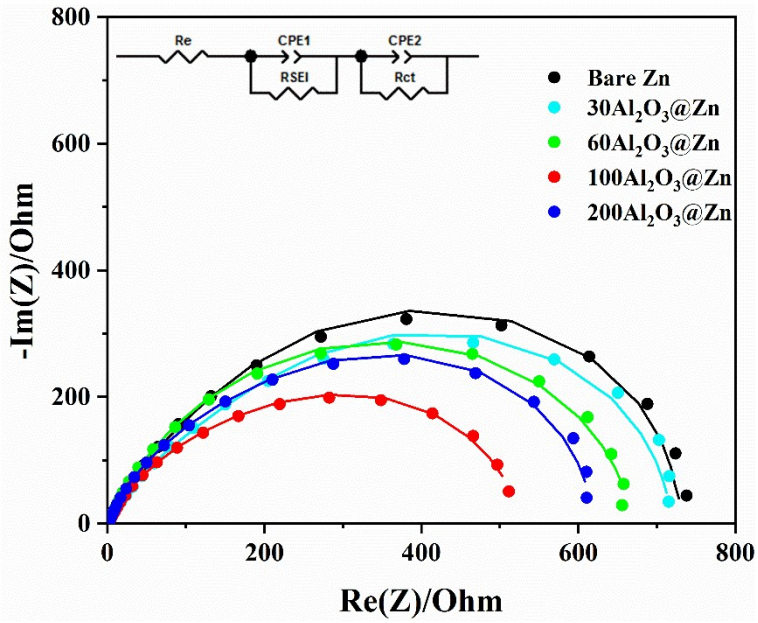

Figure S4. The Nyquist plots and fitting curve for Zn|Zn symmetric cells with bare Zn, $30Al_2O_3$@Zn, $60Al_2O_3$@Zn, $100Al_2O_3$@Zn, and $200Al_2O_3$@Zn before cycling (the inset is the equivalent circuit). The dots are the raw EIS data and the solid line are the fitting curves.

Table S1. The calculated impendence parameters for bare Zn, $30Al_2O_3$@Zn, $60Al_2O_3$@Zn, $100Al_2O_3$@Zn, and $200Al_2O_3$@Zn symmetric cells before cycling.

	Bare Zn	**$30Al_2O_3$@Zn**	**$60Al_2O_3$@Zn**	**$100Al_2O_3$@Zn**	**$200Al_2O_3$@Zn**
R_e /Ω	1.0	1.0	1.0	1.2	1.3
R_{SEI} /Ω	238.2	289.0	301.7	360.2	380.3
R_{ct} /Ω	489.2	431.2	368.1	170.8	239.8

Figure S4 shows the EIS for the Zn|Zn symmetric cells with bare Zn, $30Al_2O_3$@Zn, $60Al_2O_3$@Zn, $100Al_2O_3$@Zn, and $200Al_2O_3$@Zn before cycling. All the EIS spectra are composed of a depressed semicircle in the high to medium frequency region. Generally, the intercept of the semicircle at the Zreal-axis in the high frequency region represents internal ohmic resistance (R_e), which includes contributions from the electrolyte, current collector, and separator etc. The semicircle in the high-medium frequency is related to solid electrolyte interface (R_{SEI}) and charge transfer resistance (R_{ct}) at the electrode-electrolyte interface. For a more interpreting of the EIS results, the equivalent circuit (inset in Figure 2d) was employed for fitting the EIS data using Z-View software. The fitting line matched well with the raw EIS data, indicating the suitability of the adopted equivalent circuit. As shown in **Table S1**, the small difference of R_e among these samples indicates a negligible impact on the internal ohmic resistance by different amount of ALD Al_2O_3 coating with nanometers thickness. The R_{SEI} increase with the ALD coating cycles which may arise from the increasing thickness of Al_2O_3 coating layers. However, all the samples with ALD coating exhibited a lower R_{ct} than the bare one, suggesting that ALD Al_2O_3 coating can favor the electrode/electrolyte interface reaction. And $100Al_2O_3$@Zn shows the lowest R_{ct} value among all the samples. The EIS result agrees with the charge-discharge profiles (**Figure 2a**), and the optimized Al_2O_3 coating is with 100 ALD cycles (~ 10 nm in thickness).

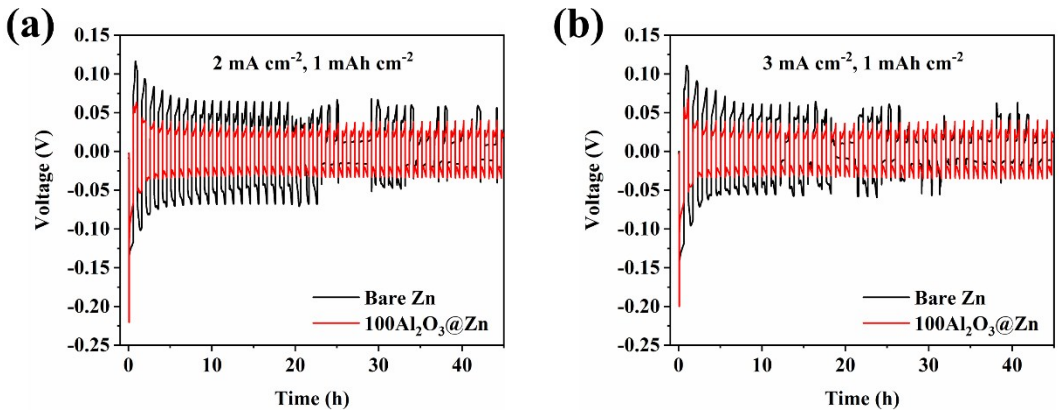

Figure S5. Zn stripping/plating ability for bare Zn and $100Al_2O_3$@Zn at high current densities of (a) 2 mA cm^{-2} and (b) 3 mA cm^{-2} with a capacity of 1 mAh cm^{-2}.

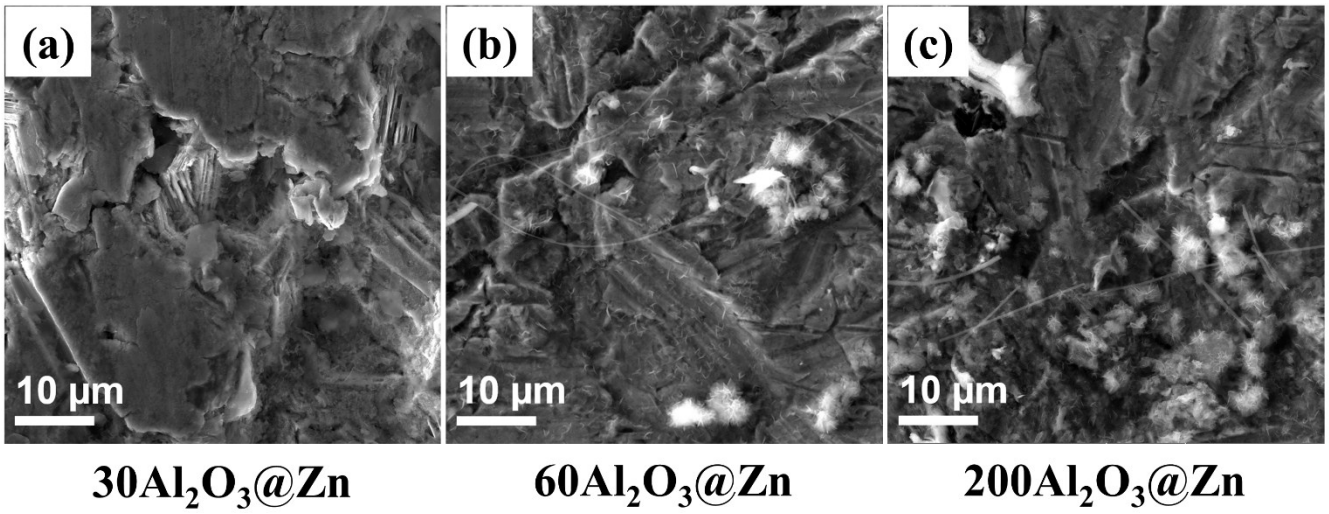

Fig. S6 The SEM images of the Zn anodes coating with different ALD cycles after cycling for 50 h. (a) $30Al_2O_3$@Zn, (b) $60Al_2O_3$@Zn and (c) $200Al_2O_3$@Zn. All the Zn|Zn symmetric cells were cycled at 1 mA cm^{-2} with a capacity of 1 mAh cm^{-2}.

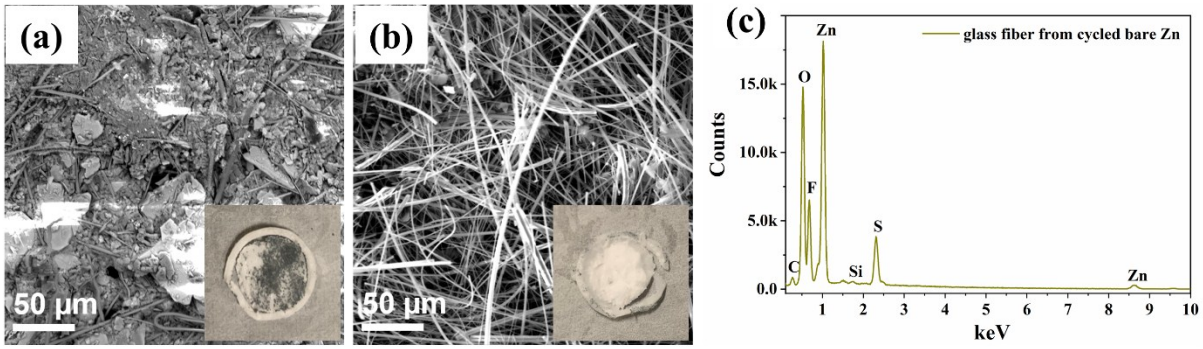

Figure S7. SEM images of the separators recovered from bare Zn (a) and 100Al_2O_3@Zn (b) symmetric cells after cycling (insert shows the corresponding optical image of the separator). (c) EDX spectrum of the glass fiber separator from the cycles bare Zn symmetric cells.

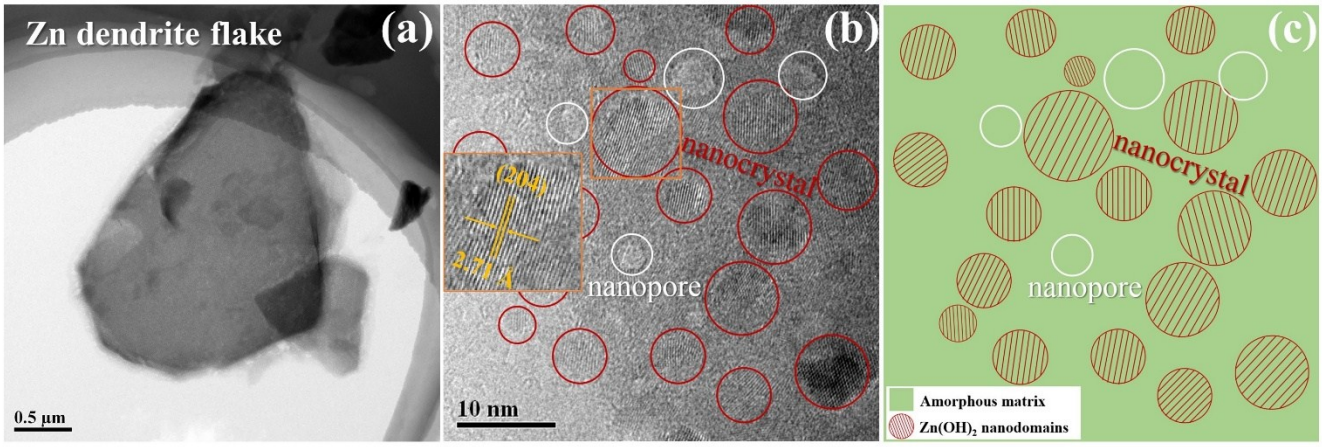

Figure S8. (a) Bright-field TEM images of a single Zn dendrite flake. (b) high-resolution TEM images (HRTEM) of the dendrite from bare Zn after cycling. (c) schematic of the observed structure of Zn dendrites.

As XRD and XPS analysis revealed the dendrites formation of $Zn(OH)_2$ in the Zn electrode after cycling, the Zn dendrites was further characterized by HRTEM characterization to support this conclusion. Before carrying out HRTEM characterization, the cycled bare Zn was intensively ultrasonicated in deionized water to collect the Zn dendrite for HETEM samples. The bright-field TEM image of a single Zn dendrite from bare Zn (**Fig. S8a**) shows the similar flake morphology as that of SEM in **Fig. 4b**. The HRTEM images (**Fig. S8b**) clearly indicate that there are many nano-crystal domains and nanopores distributed randomly into the amorphous matrix and the clear interplanar spacings can be measured as 2.71 Å (inset), which corresponds to the (204) planes of tetragonal $Zn(OH)_2$ (JCPDS No. 36-1451). The large amount of amorphous structure maybe come from the SEI (solid electrolyte interphase) component, which can be further investigated by other advanced characterizations. The schematic of the observed structure of Zn dendrites can be illustrated in **Fig. S8c**. As illustrated, the Zn dendrite flake is porous structure with nanocrystal $Zn(OH)_2$ imbedded in amorphous matrix.

Table S2 Tafel fit corrosion kinetic parameters and corrosion inhibition efficiencies of bare Zn and $100Al_2O_3$@Zn.

Samples	E_{corr} (mV)	I_{corr} (mA)	j_{corr} (mA cm^{-2})	β_a (mV dec^{-1})	β_c (mV dec^{-1})	R_p (Ω cm^{-2})	P_p (%)
Bare Zn	-871.1	8.20	5.47	248.5	249.8	9.90	—
$100Al_2O_3$@Zn	-875.7	4.91	3.27	225.8	218.8	14.77	40.12

E_{corr}: corrosion potential

I_{corr}: corrosion current

j_{corr}: corrosion current density

βa and βc: the anodic and cathodic Tafel coefficients, respectively

Rp: polarization resistance, was calculated by:

$$R_p = \frac{\beta_a \beta_c}{\ln(10)\, j_{corr}(\beta_a + \beta_c)}$$

Pp: corrosion inhibition efficiency, was calculated by:

$$P_p\% = \frac{j_{corr}^{0} - j_{corr}}{j_{corr}^{0}} \times 100$$

where j_{corr}^{0} is the value of corrosion current density of bare Zn, and j_{corr} is the value of corrosion current density of $100Al_2O_3$@Zn.

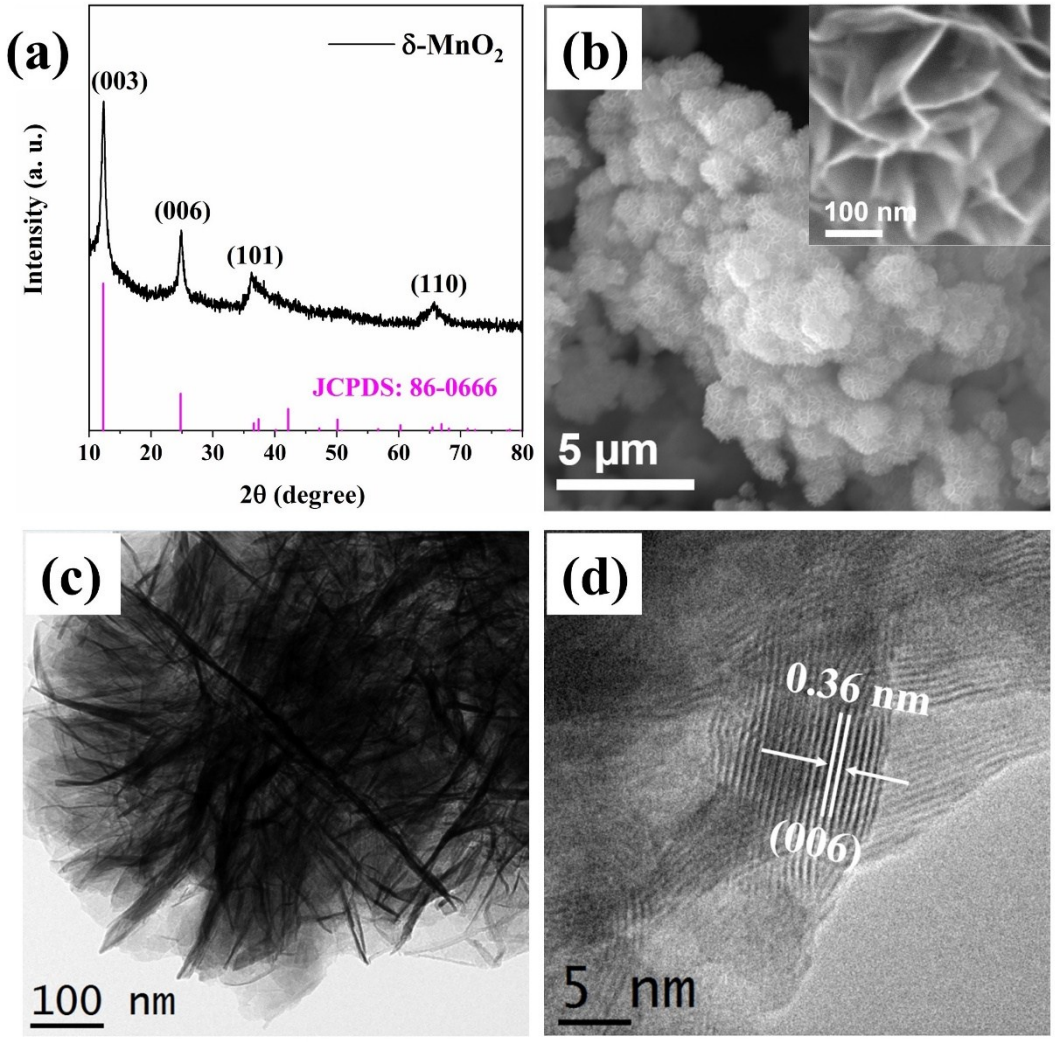

Figure S9. (a) XRD pattern, (b) SEM images, (c) TEM images and (d) HRTEM images of δ-MnO_2 cathodes.

The crystalline phase of as-prepared δ-MnO_2 was confirmed by XRD, as shown in **Fig. S9a**, which is in good agreement with the structure of layered birnessite with R-^{3}m space group (JCPDS No. 86-0666). The SEM and TEM images (**Fig. S9b, Fig. S9c**) of the as-prepared δ-MnO_2 shows three-dimensional micro/nano spheres morphologies with an average dimeter of around 2 μm, which consists of small nanosheets with thickness of around 10 nm. HRTEM images in **Fig. S9d** reveals the lattice spacing of 0.36 nm for the (006) crystal plane of δ-MnO_2.

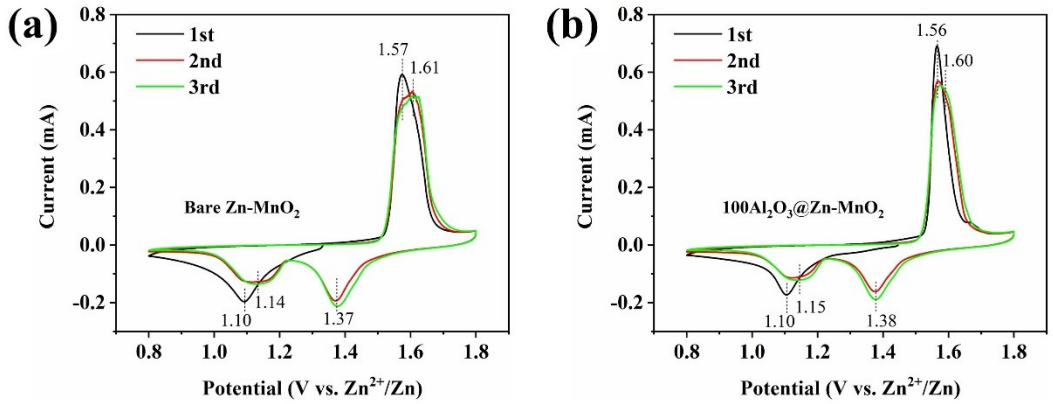

Figure S10. Cyclic voltammetry (CV) curves of bare Zn and $100Al_2O_3$@Zn for the initial three cycles at a scan rate of 0.1 mV s^{-1}

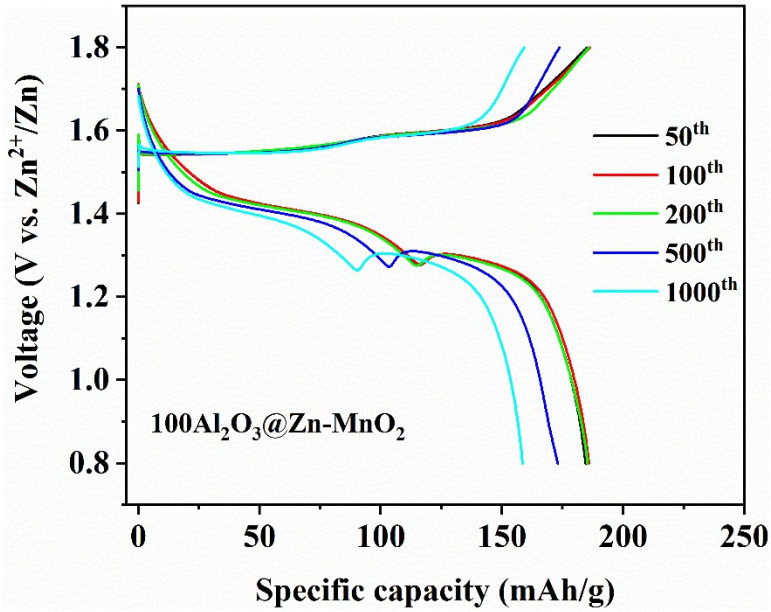

Figure S11. Charge-discharge profiles of $100Al_2O_3$@Zn for the 50^{th}, 100^{th}, 200^{th}, 500^{th}, and 1000^{th} cycles at a current density of 1 A g^{-1}.